Fédération Internationale du Béton
Proceedings of the 2nd International Congress
June 5-8, 2006 – Naples, Italy

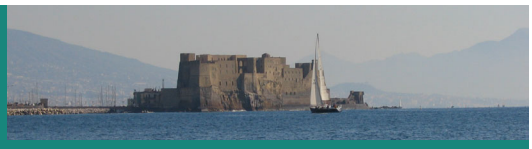

ID 8-43 Session 8 – Seismic design of new concrete structures

Study on Damage Controlled Precast-Prestressed Concrete Structure with P/C MILD-PRESS-JOINT – Part 2: Experimental Study on Mechanical Behavior of Frame with P/C MILD-PRESS-JOINT

Sakata, H., Wada, A.
Structural Engineering Research Center, Tokyo Institute of Technology, 4259-R3-18, Nagatsuta-cho, Midori-ku, Yokohama, Kanagawa, 226-8503, Japan

Nakano, K.
Nakano Building Research & Associate

Matsuzaki, Y.
Tokyo Univ. of Science

Tanabe, K.
KTB Association, Kurosawa Construction Company

Machida, S.
Tokyo Kenchiku Structural Engineers

INTRODUCTION

The PC Mild-Press-Joint method was proposed in the previous paper for controlling earthquake damage to buildings. It is expected to be effective in future seismic designs. However, there have been almost no experimental studies on PC Mild-Press-Joints. Thus, full understanding has not been gained on their mechanical characteristics. This paper reports the results of experiments [1], [2], [3] carried out on ┼- shaped frames and ├- shaped frames designed using this method. The experiments were categorized into BF-series and JS-series. The purpose of the BF-series was to determine if the PC Mild-Press-Joint had been achieved. The specific target was to clarify the basic mechanical properties such as hysteresis, joint behavior, failure, etc. The purpose of the JS-series was to clarify the shear characteristics of the frame's column/beam PC Mild-Press-Joint. This paper is aimed at obtaining basic data to establish a method for designing frames using PC Mild-Press-Joints.

Keywords: P/C MILD-PRESS-JOINT frame, ┼- shaped frame, ├- shaped frame, beam-column joint, damage control, shear strength of joint panel

EXPERIMENT PROGRAM

Specimen

Experiments were carried out on ┼- shaped frames and ├- shaped frames. They were categorized into BF-series and JS- series. The purpose of BF-series was to determine if the PC Mild-Press-Joint method had been achieved. The specific target was to clarify the basic mechanical properties such as hysteresis, joint behavior, failure, etc. The purpose of the JS-series was to clarify the shear characteristics of the frame's column/beam PC Mild-Press-Joint.
The specimen configurations and bar arrangement details are shown in Fig. 1. Specimen parameters and material properties are shown in Tab. 1. Specimens were 1/3 scale models of a commercial building. They

represented part of a framework including beam-column joints at the 1st and 2nd stories of a five-story building cut at the center of column height and beam span. The beam cross-section was: b x D = 230 x 420mm and column cross-section was: b x D = 320 x 320 mm. The parameters for the frame experiments for the ┼- shaped part in the BF-series were the frame structure (PC Mild-Press-Joint method or RC frame), presence or absence of corbel in PC specimens and wiring pattern of prestressing strands. Those in the JS-series were the frame structure, strength of concrete column and number of prestressing strands. The ├- shaped frame experiments employed only one PC specimen for the BF-series and one each for the PC and RC specimens for the JS-series. A total of 11, i.e. eight and three specimens, were used for the ┼- shaped frame and the ├- shaped frame, respectively. Nos.1 through 4, 9 and 10 were assigned for the BF-series. Nos.5 through 8 and No.11 were for the JS-series. Nos.4 and 7 were RC specimens (monolithic structure). The bending strength of No.4 specimen was made equal to that of No.3 specimen. That of No.7 was made equal to those of Nos. 5 and 6. That of No.10 was made equal to that of No. 9. Nos.8 and 11 were reinforced by winding the steel plate on beam ends and corbel to protect them from crushing. The specimen parameters and material characteristics are shown in Tab.1. Settings for beam shear span-to-depth ratio 3.0 and column shear span-to-depth ratio 2.2 were made common for all the test pieces. In each PC specimen, prestressing strands were placed in two rows on the beam cross-section, and the main beam bars (normal reinforcing bars) did not penetrate the joint panel. The beam flexural strengths of each of them were made the same as those of the PC specimen in the BF-series and JS-series. The column bending strengths of all the cross-shaped specimens were about 1.4 times the beam bending strengths. The shear margin of both column and beam was about 1.7. Column bending strengths of all the ├- shaped specimens were over 3.3 times the beam bending strengths. The shear margins of beam and column were about 1.7 and over 1.1, respectively.

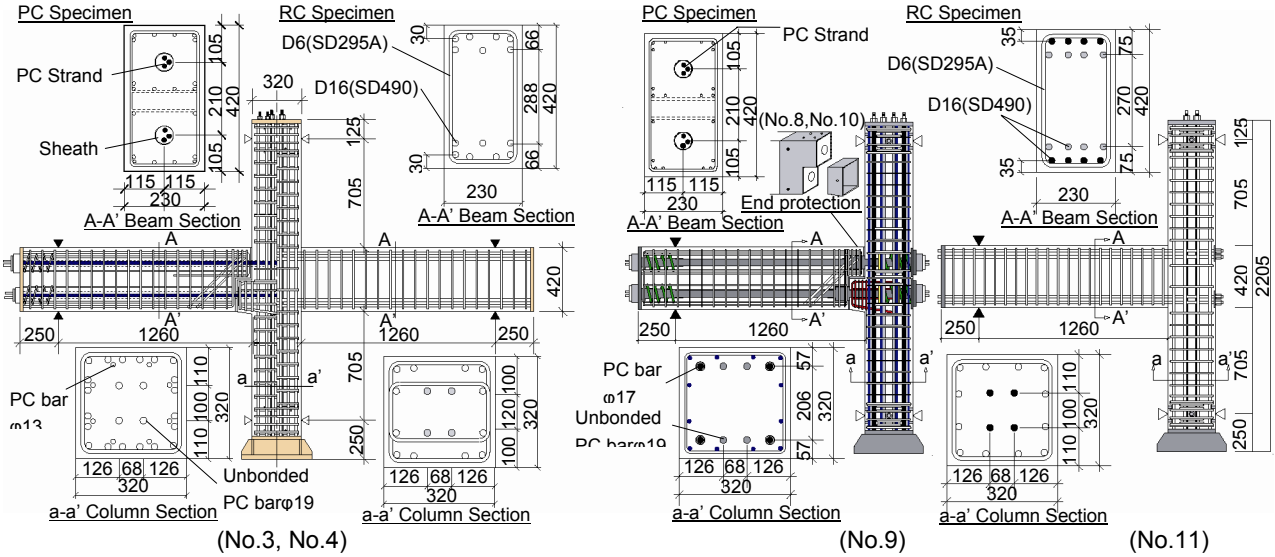

Fig. 1. Specimens

Table1. Parameters of Specimen and Material Properties

	Specimen No.	Name	Series	Number of Strand (Main Reinforcement) Upper	Lower	Corbel	$_cσ_B$ beam/column N/mm^2	E_c beam/column kN/mm^2	$_cσ_t$ beam/column N/mm^2	$_pσ_y$ ($_sσ_y$) N/mm^2	E_p (E_s) kN/mm^2	$σ_p$ beam/column N/mm^2
				Number of Strand								
┼-shaped	1	┼-PC42-C-90	BF	4	2	○	92.0	44.6	4.3	1762	214	4.8/3.8
	2	┼-PC42-N-90		4	2	×	92.4	43.6	3.5			
	3	┼-PC33-C-90		3	3	○	87.5	43.1	3.3			
	4	┼-RC33-50		7-D16	7-D16	-	58.0	37.0	3.5	(357)	(197)	-
	5	┼-PC55-C-90	JS	5	5	○	91.5	42.5	3.9	1628	212	8.1/3.8
	6	┼-PC55-C-50		5	5	○	86.3/55.8	40.4/35.2	3.8/3.3			
	7	┼-RC55-50		7-D16	7-D16	-	56.8	37.2	3.2	(538)	(193)	-
	8	┼-PC66-C-90		6	6	○	89.9	43.3	5.0	1667	216	9.7/3.8
├-shaped	9	├-PC33-C-90	BF	3	3	○	92.1	44.2	4.2	1663	216	5.46/3.8
	10	├-PC66-C-50	JS	6	6	○	90.7/61.7	43.1/39.2	3.5/3.2	1663	216	10.7/3.8
	11	├-RC66-50		8-D16	8-D16	-	55.5	38.9	3.6	(358)	(197)	-

*1: PC Strand (SWPR7B),*2: SD295A,*3: SD490, BF-Series: beam yield preceding type, JS-Series: suffered larger shear force in joint panel $_cσ_B$: Concrete Compressive Strength, E_c: Concrete Young's Modulus, cσt: Concrete Tensile Strength, pσy: Strand Yield Strength (0.2%offset), $_sσ_y$: Beam Main Reinforcement Yield Strength, E_p: Strand Young's Modulus, E_s: Beam Main Reinforcement Young's Modulus

Experimental Method

The loading apparatus for the ┼ shaped frame and loading cycle are shown in Fig. 2. A shear force was applied to the right and left beams using two 490(kN) hydraulic jacks, as shown in Fig. 2. The vertical displacements at the loading point were controlled to keep them same when the shear force was applied. The cyclic loading was increased according to the loading cycle shown in Fig.2. For the ┼ shaped frame, an axial force of about 745 kN (axial force ratio =0.08 [Fc: 90 N/mm^2], =0.15 [Fc: 50 N/mm^2]) was applied to the column using an unbonded prestressing rod built into the column member. For the ├ shaped frame, the axial force was half.

Jack load, displacement, steel member strain and crack width were measured. The widths of cracks across the shear reinforcing bars where strain gauges were attached were measured for the JS-series at the time of peak story drift angle using a digital microscope with a minimum scale of 0.01mm.

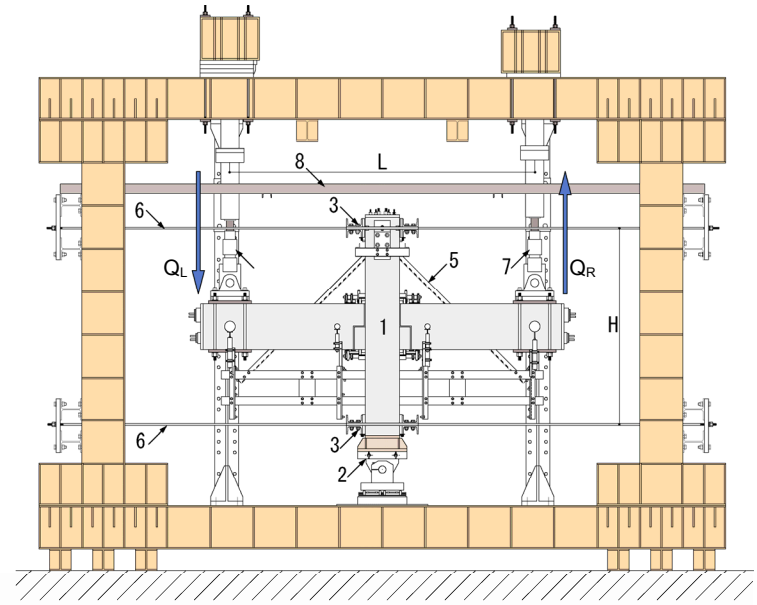

1:Specimen, 2:Pin-roller, 3:Column pin support aparatus,
4:490kN oil jack, 5: Holder for displacement measurement,
6:PC bar, 7:Load cell, 8:Lateral deformation binding channel

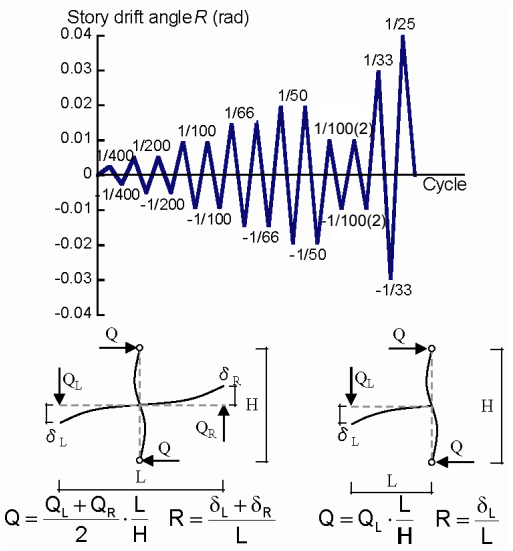

Q_L: Left beam shear force
Q_R: Right beam shear force
δ_L: Vertical displacements at Left beam loading point
δ_R: Vertical displacements at Right beam loading point

Fig. 2. Loading Apparatus and Loading Cycle

EXPERIMENT RESULT AND DISCUSSIONS

Characteristics of Failure and Deformation

BF-Series

Figs. 3(a)-(d) shows the part near the beam-column joint at the time of maximum deformation. Figs. 4(a)-(d) shows the relationship between story shear Q and story drift angle R. As shown in Fig. 4, the PC specimen (Nos. 1 through 3 and 9) indicated linear initial stiffness. Thereafter, clearance occurred at the press joint (connection) part when prestress was cancelled (No. 1: R= 1/100 rad.) at the tension edge of the beam ends. Then, stiffness decreased. Up to that point, no bending cracks were observed in the general parts of the column and beam members. After story deformation angle reached R = 1/66 rad., the strength almost leveled off due to beam bending yield. No residual deformation occurred until about R = 1/100 rad. and thereafter, origin-oriented hysteresis characteristics were observed. The joints in the above process showed elastic behavior where joint clearance occurred due to the prestressing strands extending from the beam-column joint, and the clearance closed due to press binding prestress when load was released. No large difference was observed due to wiring of the prestressing strands (Nos.1 and 3) or the presence of a corbel (Nos.1 and 2). Almost no damage was observed in the PC specimens (Nos. 1 through 3 and 9) until about R = 1/100 rad. Thereafter, concrete cracks and joint mortar separation were concentrated at and near joints, and no residual cracks were observed in general parts of beam and column members. While no difference was observed for different specimen configurations (┼

shaped and ├- shaped), the maximum shear forces in the ├- shaped specimens were about half of those in the ┼- shaped specimens for identical wiring of prestressing strands. Meanwhile, the RC specimen (No. 4) showed cracking at the beam members at about R= 1/1600 rad. and decreasing stiffness. After both beam main 1st level and second level reinforcing bars yielded at R= 1/100 rad., the joint's shear reinforcing bars yielded. Thereafter, shear cracks extended at the joints, followed by shear failure (R= 1/66 rad.). Cracks were observed all over the beam and column members and joints. Hysteresis was spindle-shaped type up to R = 1/66 rad., and then changed to slip type as joint damage increased. As a result, it was interpreted that setting of prestressing strand at 0.5Py enabled elastic extension of prestressing strand, generated elastic rotational behavior (elastic rotation) of the joint and concentrated damage at the joints.

JS-Series

Concrete of the beam end compression side started separating at about R = 1/100 rad. in ┼- shaped specimens No. 5 (column Fc = 90 N/mm^2) and No. 6 (column Fc = 50 N/mm^2), where five prestressing strands were placed at each upper and lower level. Then, they reached bending compressive failure at the beam end when R = 1/66 rad. Meanwhile, ┼- shaped specimen No.8 (column Fc = 90 N/mm^2) and RC specimen No. 7 (column Fc = 50 N/mm^2), where the beam ends were reinforced, showed shear failure as expected. Shear reinforcing bars of the joint of No. 6 (column Fc = 50 N/mm^2) yielded at R = 1/66 rad. The beam end reached bending compressive failure at the same cycle. Thereafter, no significant strain increase was observed. The shear reinforcing bars of the joint of No. 8 (column Fc = 90 N/mm^2), where the beam end was reinforced, yielded at R = 1/100 rad. Thereafter, shear cracks at the joint rapidly extended and the joint reached shear failure at R = 1/66 rad. (2nd time). Although No.8 showed spindle-shaped hysteresis as the joint damage progressed, no rapid decrease in strength was observed (Fig. 4(c)). The prestressing strands yielded at R = 1/66 rad., but the shear reinforcing bars of the joint did not yield in ├- shaped specimen No. 10, where the beam end was reinforced. Meanwhile, after the shear reinforcing bars in the ┼- shaped specimen No. 7 (RC specimen, Fc = 50 N/mm2) yielded, shear cracks of the joint extended and shear failure was reached at the joint. Hysteresis was spindle-shaped type up to R = 1/66 rad., and then changed to slip type (Fig.-4(d)). The beam end and general part showed bending cracks and decreasing stiffness for the ├- shaped specimen No. 1. Then, after both main 1st level and 2nd level reinforcing bars yielded at R = 1/100 rad., the shear reinforcement of the joint yielded. Thereafter, shear cracks of the joint extended and shear failure was reached at the joint (R = 1/66 rad.)

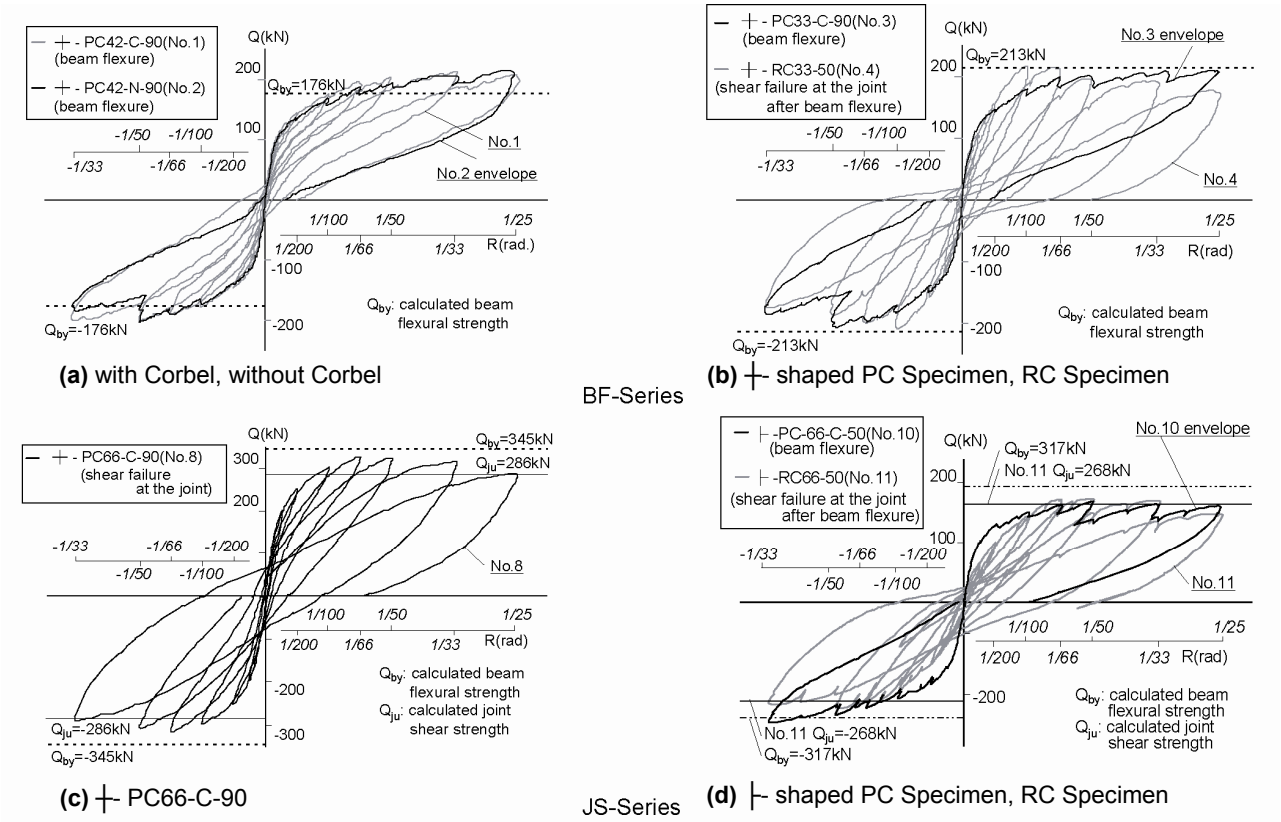

Fig. 3. Story Shear Force Q - Story Drift Angle R Relationship

Conditions of Joint Damage

Fig. 5(a) shows the sum of crack widths at peak story drift angle at the joint. Fig. 5(b) shows the sum of the widths of residual cracks. As the crack widths in the joint increased, the strain of the shear reinforcing bars of the joint increased. Comparison was made between ┼- PC55-C-50 and ┼- RC55-50 and between ├- PC66-50 and ├- RC-66-50 in the JS-series. The crack width in the joint of the PC specimens, i.e. both ┼- shaped specimen and ├- shaped specimen, was about 1/10 and 1/40 at the peak cycle and at the load-release cycle, respectively. This indicates that more cracks closed in the PC specimen than in the RC specimen during unloading.

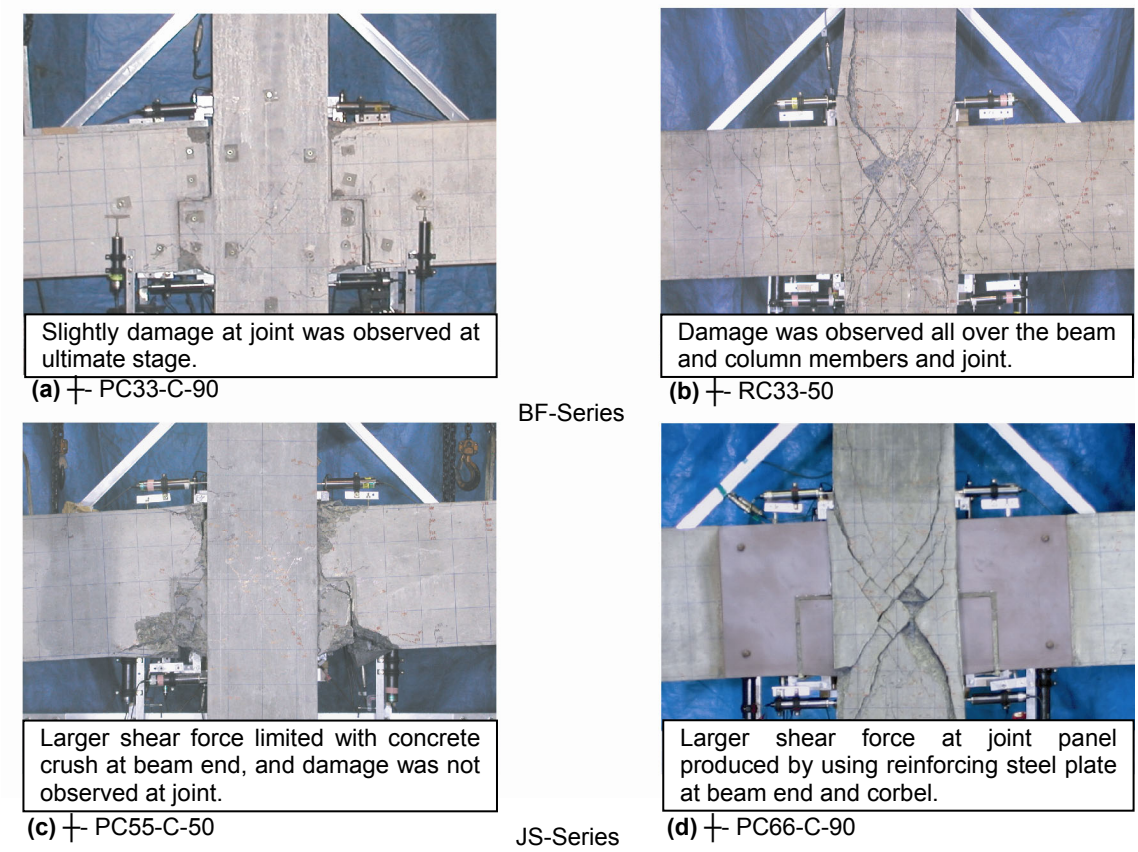

Fig. 4. Ultimate Stage (R=1/25 rad.)

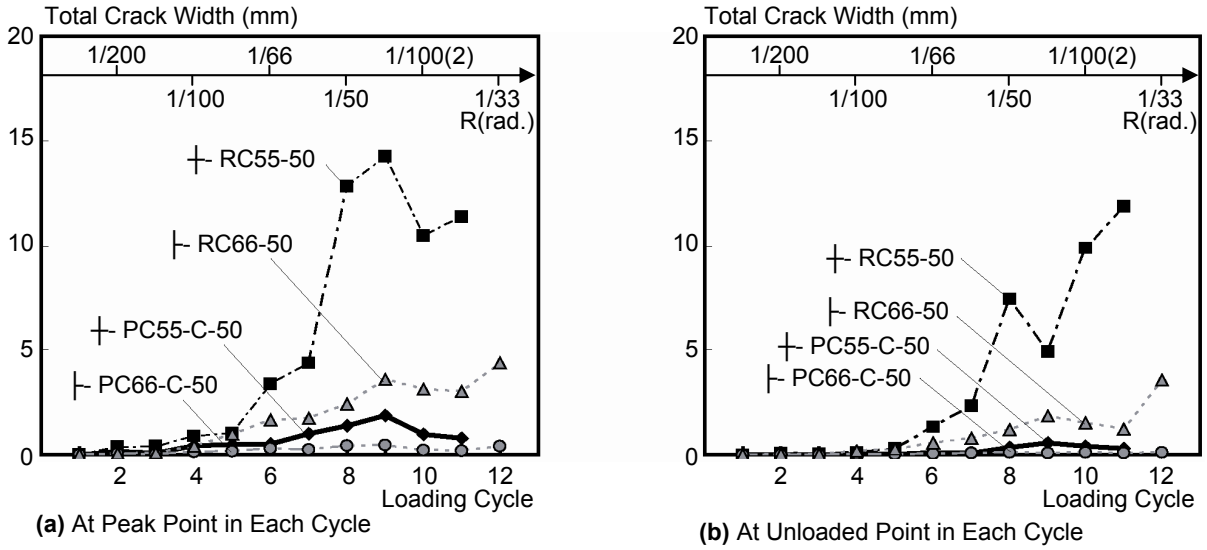

(a) At Peak Point in Each Cycle

(b) At Unloaded Point in Each Cycle

Fig. 5. Summation of Crack Width of Each Cycle

Change in location of joint rotation center

Elastic rotation of the joint, which is a characteristic point of this method, is verified. The behavior of the left beam end at the positive loading peak against the column is shown in Fig. 6. This shows horizontal and vertical relative positions of three measured points at the left beam end shown in Fig. 6(c). Three relative positions were located on almost a straight line and the beam end mainly near the compressive edge was deformed as a rigid body. Fig. 7(a) shows the changes in location of the rotation center of the left beam end in the BF-series. Specimens of ┼ PC42-C-90, ├ PC42-C-90 with a corbel showed stable changes in the location of the rotation center near the compressive edge compared with specimens of ┼ PC42-C-90 without a corbel.

Joint rotation angle

Fig. 7(b) shows ratio θ/R for joint θ rotation angle for story deformation angle R during positive peak loading for the BF-series. As shown, joints occupied a large part of the deformation in the PC specimens (Nos. 1, 2 and 9). Thus, it is interpreted that elastic rotation of the joint caused the deformation to be concentrated at the joints, and limited the concrete cracks and joint mortar separation. This resulted in damage control by suppressing cracks in the general parts of the column and beam members. Extension of the prestressing strands generated tee elastic rotation of the joint. Thus, it is considered that frame deformation can be evaluated by understanding the bond characteristics of prestressing strand.

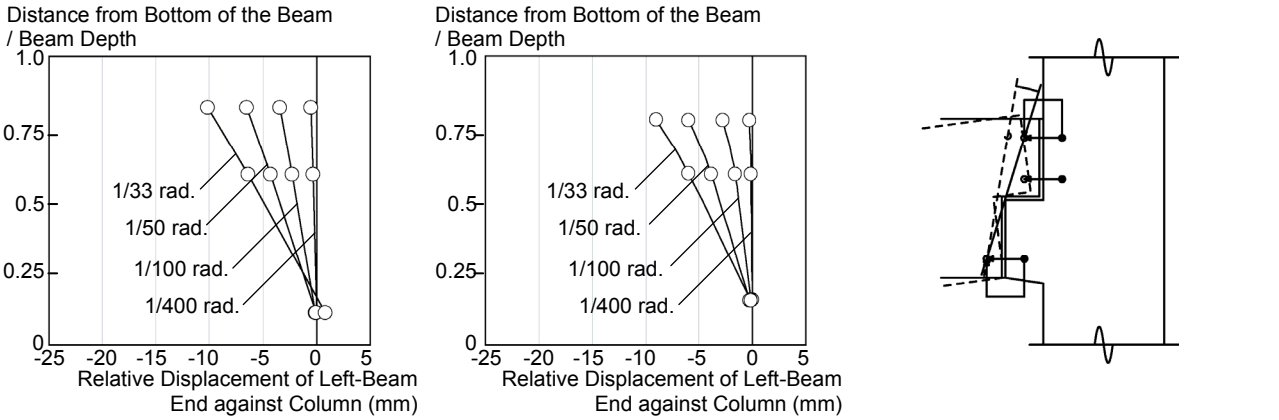

(a) ├ PC33-C-90 **(b)** ┼ PC33-C-90 **(c)** Measured Points for Relative Positions of the Left Beam

Fig. 6. Behavior of the Left Beam End against the Column

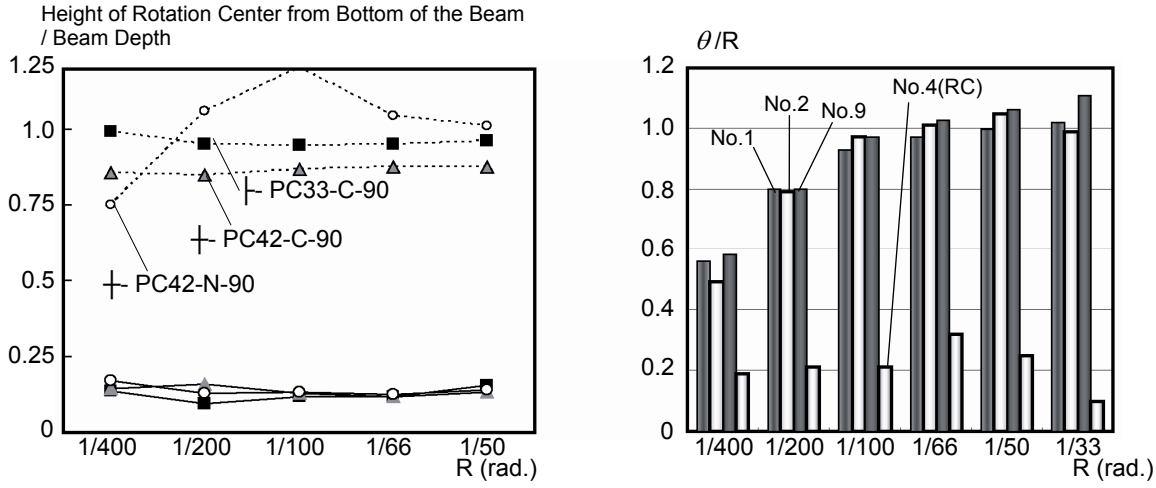

(a) Changes of Location of the Rotation Center of the Left Beam end **(b)** Ratio θ/R for Joint θ Rotation Angle for Story Drift Angle R

Fig. 7. Behavior of the Rotation of the Joint

Strain Characteristics of Prestressing Strand

Fig. 8(a) shows the strain distribution (during positive loading) up to R = 1/100 rad. for Nos. 7 and 8. Fig.8 (b) shows that for Nos. 10 and 11. The solid and dashed lines in Figs. 8(a) and (b) show strain distribution of the prestressing strands at the upper level and that of the main reinforcing bars at the 1st level beam, respectively. The strain distribution of the prestressing strands showed a more gentle strain gradient than ordinary reinforcing bars, showing that they have a smaller bond stress. The strain distribution in the ┼- shaped prestressing strands showed a symmetrical triangular shape having a vertex at the location of the critical section with a large bond length. The strain distribution of the ├- shaped PC specimen showed a near trapezoidal shape, where the distribution was cut at the bond fixture side of the prestressing strands in the column.

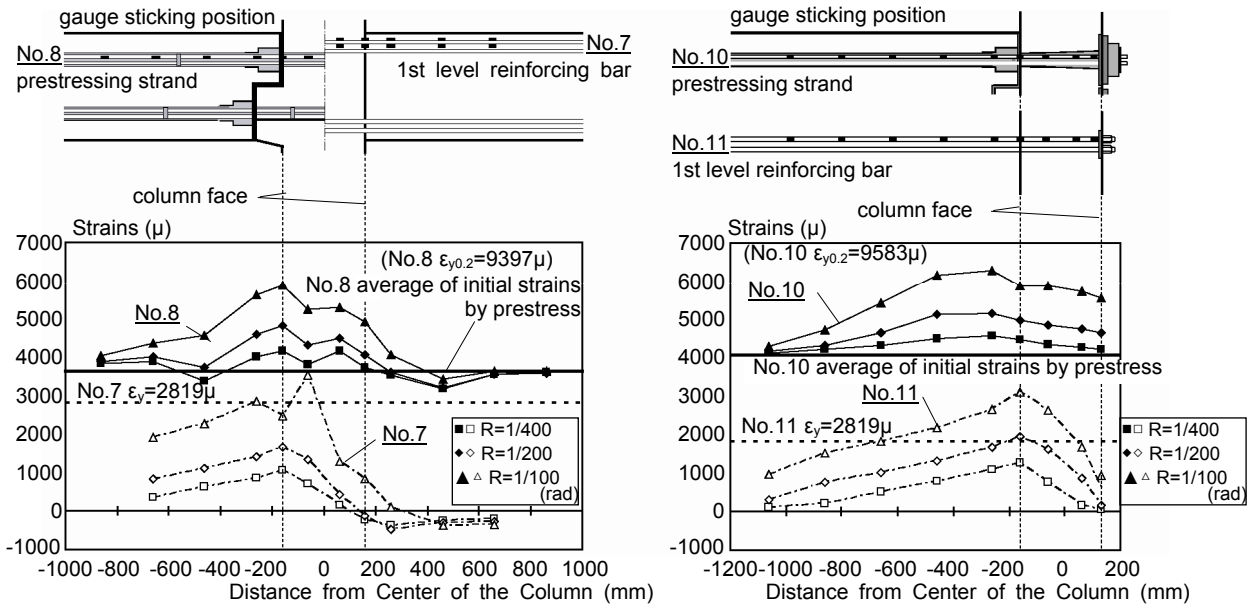

(a) No.7 (┼- RC66-50), No.8 (┼- PC66-C-90) **(b)** No.10 (├- PC66-C-50), No.11 (├- RC66-50)

Fig. 8. Strain Distribution of Prestressing Strand and Main Reinforcing Bar

MODELING OF ENVELOPE

The *Q* – *R* relationship envelope for the frame using a PC Mild-Press-Joint was modeled. It was assumed that the envelope moved to secondary stiffness during release of the initial press binding and that it should become tri-linear when the stiffness became zero when the frame reached yield. The first inflection point in the envelope was shown to be at the intersection of the initial stiffness and the moment when release of press binding occurred. The initial stiffness was calculated by taking into account only bending deformation, assuming the stiffness region specified in RC standard [4] in the beam-column joint at the ┼- shaped part of the frame. The moment at press binding release (the first inflection point in the envelope) M_1 was calculated from equation (1). This is the moment when a force equivalent to the initial force was applied to the tensile side of the prestressing strands. M_1 was converted to the story shear force Q_1 by equation (2).

$$M_1 = \Sigma T \cdot j = A_p \cdot E_p \cdot \varepsilon_{pini} \cdot j \quad (1)$$

$$Q_1 = \frac{M_1}{a} \cdot \frac{L}{H} \quad (2)$$

where [A_{pt}: cross-sectional area of tensile side of prestressing strand, E_p: Young's modulus for prestressing strand, ε_{pini}: initial strain of prestressing strand at time of anchoring, j: distance between tension and compression resultants (=7/8d, d: Effective depth), a: shear span, L: beam span, and H: elevation between stories]

Next, the second inflection point in the envelope was obtained. It was assumed that the strain in the tensile side prestressing strand was the strain for 90% of the load against 0.2% permanent elongation in the tensile

test for the prestressing strand. The moment M_2 at the second inflection point in the envelope was calculated by setting $\varepsilon_{pt} = \varepsilon_{pini} + \Delta\varepsilon_p = \varepsilon_{0.9}$ in equation (1). Distance between tension and compression resultants was calculated using equilibrium equation considering initial strain ε_{ini} in strand. Popovics's model was used for stress-strain relationships of concrete and we assumed that concrete strain at the position of tension strand is 8000μ taking account of the strain gap between concrete and strand. Story drift angle at the second inflection point R_2 in the envelope was obtained from equation (4), (4'), where the rotation angle of the press joint was obtained from equation (3). It was judged that equation (3) could be applied to the frames using the PC Mild-Press-Joints. This is because the deformation due to the rotation angle of the press joint occupied almost 100% of the story drift angle for the region larger than R =1/100 rad. Also, δ_2 as an extracted quantity of then prestressing strands was obtained from equation (5), (5'). Fig. 9 shows the strains of PC strands and bond slip displacement.

$$\theta_2 = \frac{\delta_2}{\alpha} \tag{3}$$

$${}_{+PC}R_2 = \frac{2(\theta_2 \cdot a)}{L} \tag{4}$$

$${}_{\vdash PC}R_2 = \frac{\theta_2 \cdot a}{L} \tag{4'}$$

$${}_{+PC}\delta_2 = 2\int \varepsilon(x)dx = \Delta\varepsilon_p \cdot l_x \tag{5}$$

$${}_{\vdash PC}\delta_2 = \Delta\varepsilon_p \cdot \left(\frac{l_x}{2} + D\right) \tag{5'}$$

where [α: distance from the neutral axis to the tensile side prestressing strand, ${}_{+PC}/{}_{\vdash PC}\delta_2$: extract quantity of prestressing strand in the $+$ shaped/ $\vdash$ shaped frame, $\Delta\varepsilon_p$: incremental strain of prestressing strand on the beam-column interface, and D: column height]

Bond length l_x is defined by equation (6).

$$l_x = \frac{\Delta\varepsilon_p \cdot E_p \cdot A_p}{\tau_{ave} \cdot \phi} \tag{6}$$

where [τ_{ave} : τ_{ave}=1.42 N/mm^2 from the average bond stress of the prestressing strand and grout material, and ϕ : periphery of prestressing strand surface (= 53.34 mm)]. Average bond stress was set to τ_b=1.42 N/mm^2 derived from strain distribution of strand at R=1/100 rad. as shown in Fig. 8.

Fig. 10 shows skeleton curves for specimens $+$ PC33-C-90 and $\vdash$ PC33-C-90 in the relationship of story shear force – story deformation angle obtained from the above. They are considered capable of evaluating experimental results in general.

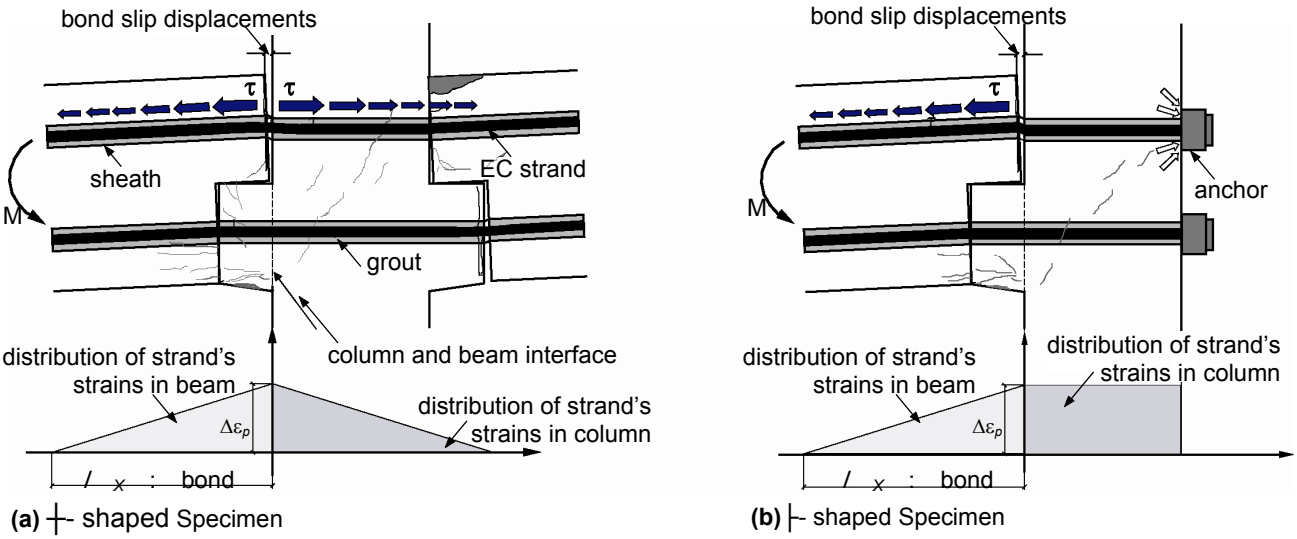

Fig. 9. Strains of PC Strands and Bond Slip Displacement

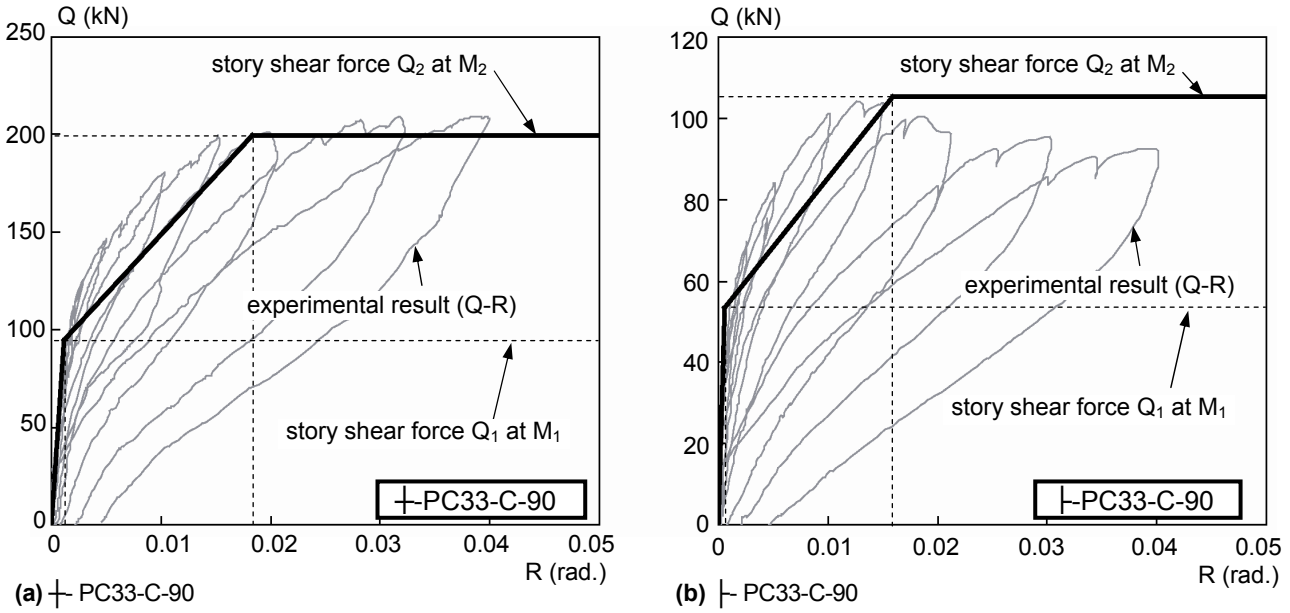

Fig. 10. Experimental Results and Tri-Linear Skelton Curve

STUDIES ON JOINT STRENGTH

Shear Crack Strength of Joint Panel

To study the strength of the joint, its shear crack strength ${}_{ex}\tau_{cr}$ during the experiments was first estimated. ${}_{ex}\tau_{cr}$ was obtained from equation (7). V_{jcr} is the shear force input to the joint when the crack first occurs at the joint, as obtained from equation (8). The tensile force was obtained from equation (9). The shear crack strength of the joint of the RC specimen was obtained from equation (10).

$$ {}_{ex}\tau_{cr} = \frac{V_{jcr}}{b_j D_j} \tag{7}$$

$$ V_{jcr} = 2T - V_c \tag{8}$$

$$ T = \frac{M_b}{j} = \frac{Q_b \cdot a}{j} \tag{9}$$

$$ {}_{RC}\tau_{cr} = \sqrt{f_t^{\,2} - \sigma_0 f_t} \tag{10}$$

where [b_j: effective joint width, D_j: column height, T: tensile force of prestressing steel or tensile force of normal reinforcing bar, V_c: column shear force (story shear force), M_b: moment at beam end, Q_b: beam shear force, a: shear span, j: distance between tension and compression resultants (= 7/8 d, d: Effective depth), f_t: tensile strength of concrete, and σ_0: column axial stress]

${}_{ex}\tau_{cr}$ obtained from equation (7) and ${}_{RC}\tau_{cr}$ obtained from equation (10) are shown by solid lines in Fig. 11. ${}_{ex}\tau_{cr}$ and values obtained from equation (10) were compared. The RC specimens showed general agreement with equation (10). However, ${}_{ex}\tau_{cr}$ for all PC specimens were larger than those obtained from equation (10). The shear crack strength in the PC specimens was evaluated using ${}_{PC}\tau_{cr}$, showing that the shear crack strength incorporated the beam prestress. ${}_{┼PC}\tau_{cr}$ was obtained from equation (11). The ├- shaped specimens had prestressing strands. Thus, taking into account the smaller area compressed by the prestress of the joint than in the ┼- shaped specimens, it was estimated from equation (11') incorporating 50% of the beam prestress force for simplicity. The concept of constraint effects by prestress force in the PC specimen is shown in Fig. 12.

$$ {}_{+}{}_{PC}\tau_{cr} = \sqrt{f_t^2 - (\sigma_0' + \sigma_p)\cdot f_t + \sigma_0' \cdot \sigma_p} \quad (11) $$

$$ {}_{\vdash}{}_{PC}\tau_{cr} = \sqrt{f_t^2 - (\sigma_0' + 0.5\sigma_p)\cdot f_t + \sigma_0' \cdot 0.5\sigma_p} \quad (11') $$

where [f_t: tensile strength of concrete, σ_0': axial stress of column taking into account column prestress, σ_p: stress due to beam prestress (BF-series: σ_p =4.02N/mm^2, JS-series: σ_p =7.61N/mm^2)]

The shear crack strength ${}_{PC}\tau_{cr}$ calculated from equation (11), (11') is shown by a dashed line in Fig. 11. ${}_{ex}\tau_{cr}$ of the PC specimen was compared with that from equation (11), (11'). The experimental results show general agreement with the calculated results.

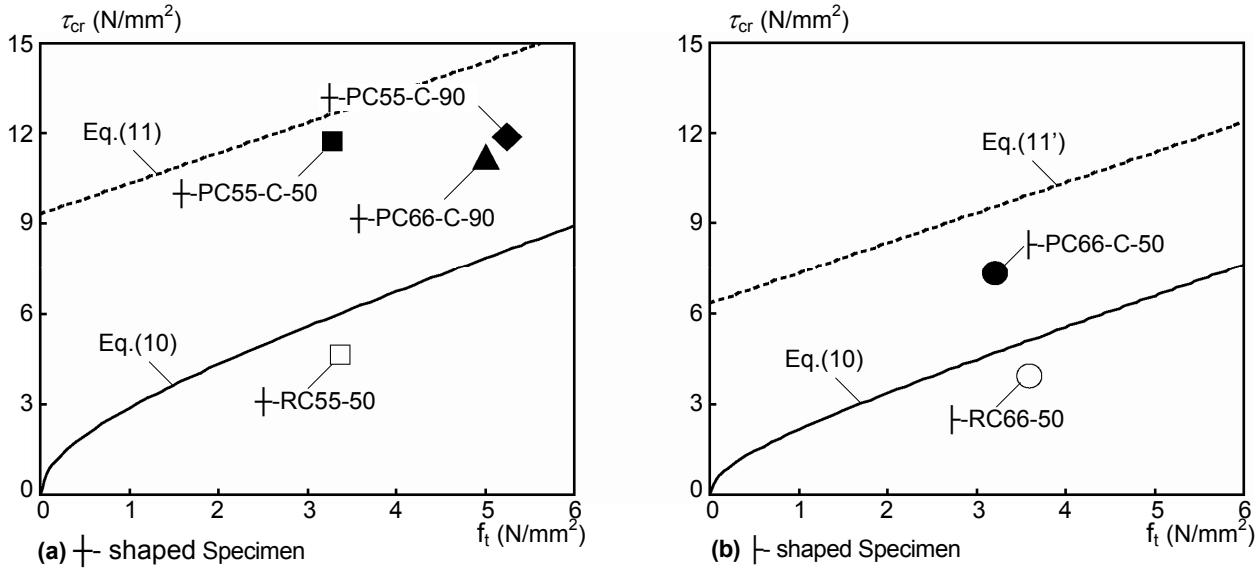

Fig. 11. Shear Crack Strength

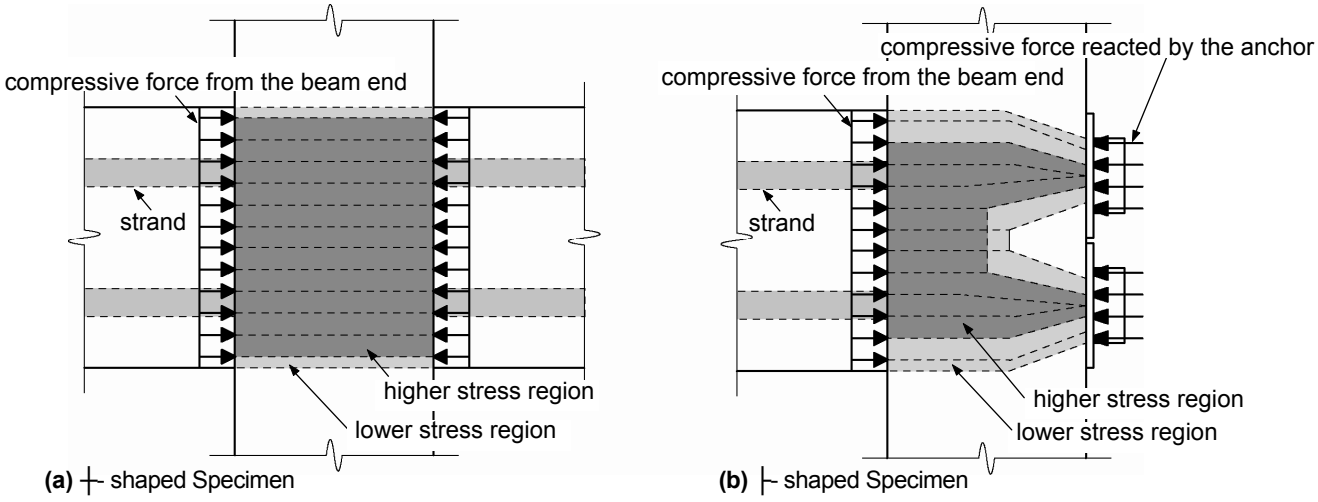

Fig. 12. Constraint Effects by Prestress Force

Shear Strength of Joint Panel

Next, the joint strength was investigated for the JS-series specimens. The joint strength during the experiments was obtained from equation (12). V_{jmax} is the maximum shear force input to the joint during the experiments. It was obtained using the same method as for V_{jcr}. The joint shear strength was obtained from equation (13).

$$ {}_{ex}\tau_{jmax} = \frac{V_{jmax}}{\kappa \cdot \phi \cdot b_j \cdot D_j} \tag{12} $$

$$ F_j = 0.8\sigma_B^{0.7} \tag{13} $$

where [κ: shape factor of joint (κ = 1.0), ϕ: correction factor according to whether there are orthotropic beams or not (ϕ= 0.85), σ_B: compressive strength of concrete]

Fig. 13 shows experimental results ${}_{ex}\tau_{jmax}$ of the ┼ shaped and ├ shaped RC specimens correspond to the calculated results in which the joint shear failure occurred. However, the shear stress at the maximum strength of ┼ shaped and ├ shaped PC specimen are higher than that estimated from previous evaluation equations, except for ┼ PC55-C-90. Thus, these evaluation equations give conservative results. It supposes that three PC specimens which show flexural yielding at beam end have larger shear strength of joint panel. Accordingly, it is found that these equations give conservative evaluation for the shear strength of the joints panel in the PC specimens.

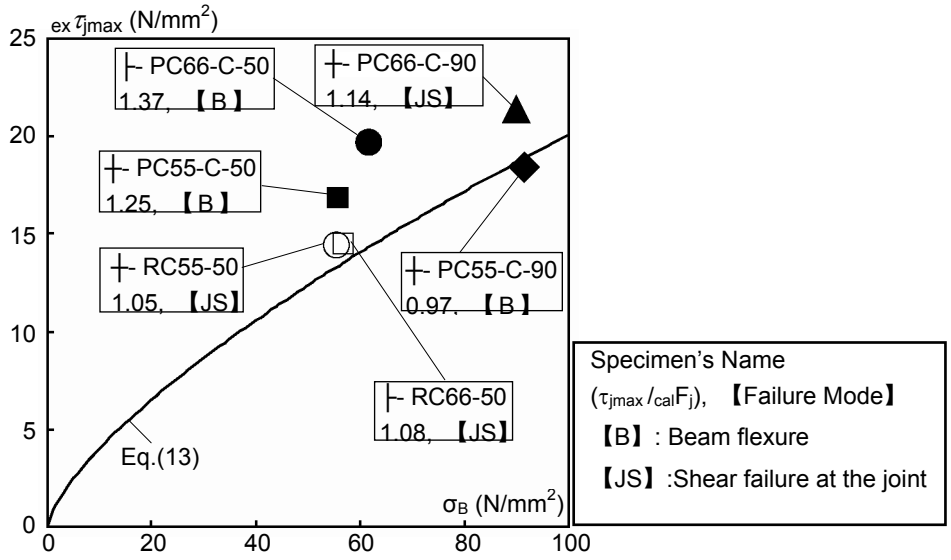

Fig. 13. Shear Stress in the Joint Panel at the Maximum Strength

CONCLUSIONS

The following conclusions were drawn from the study where partial frame experiments were conducted using prestressing strands, and verification was obtained by comparison with RC frames.

1) Hysteresis characteristics of the frame using the P/C Mild-Press-Joint were noted. Extremely small residual deformation showed high restoration capability.

2) Damage was limited to the part near the beam column interface. Damage could be controlled.

3) Shear crack strength of the joint could be evaluated by taking into account the beam prestress. Shear crack strength of ├ shaped PC specimens contributed less to the strength against the prestress force than that of ┼ shaped specimens.

4) Higher shear strength of the joint due to anchoring force can be expected for PC specimens than for the RC specimens.

5) The envelope of stiffness and strength of the frames with P/C Mild-PRESS-JOINTS could be modeled using the proposed method.

REFERENCES

1. Nakano, K., et al. Experimental Study on Mechanical Behavior of Damage Controlled Precast-Prestressed Concrete Structure with P/C Mild-Press-Joint. Journal of Structural and Construction Engineering. 2004; 10(576):125-132 (in Japanese).
2. Sakata, H., et al. Experimental Study on Beam-Column Joint of Damage Controlled Precast-Prestressed Concrete Frame with P/C Mild-Press-Joint. Journal of Structural and Construction Engineering. 2005; 2(588):141-147 (in Japanese).
3. Okano, H., Matsuzaki, Y., Sakata, H., Ikezawa, M. Structural Performance of Damage Controlled Precast-Prestressed Concrete Frame with MILD-PRESS-JOINT. Proc. of 27th Japan Concrete Institute, June 2005, Nagoya (in Japanese).
4. Architectural Institute of Japan, All Standard for Structural Calculation of Reinforced Concrete Structures -Based on Allowable Stress Concept- revised 1999, (in Japanese).